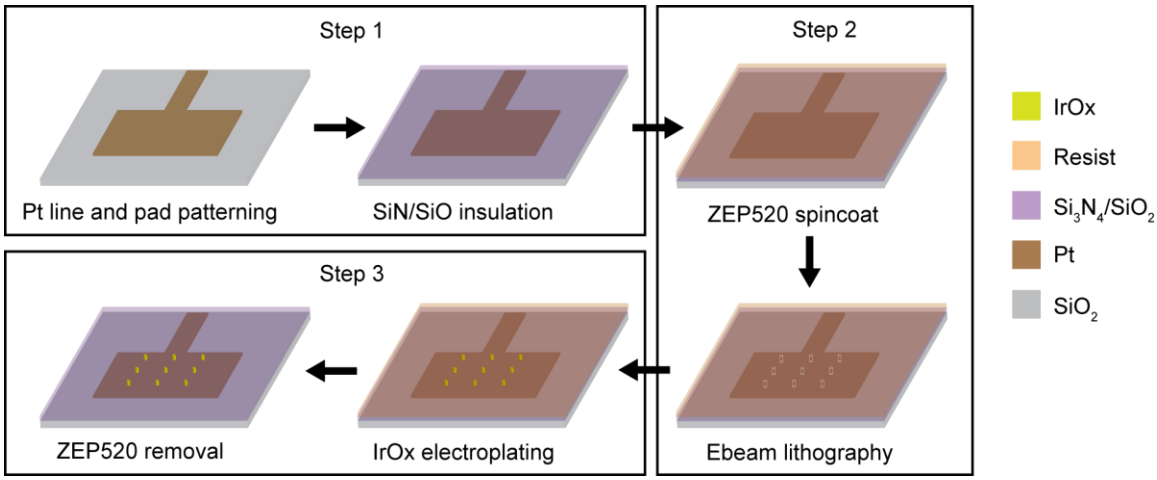

Supplementary Figure 1 | Schematics of iridium oxide nanotube electrode fabrication. See Methods for fabrication details.

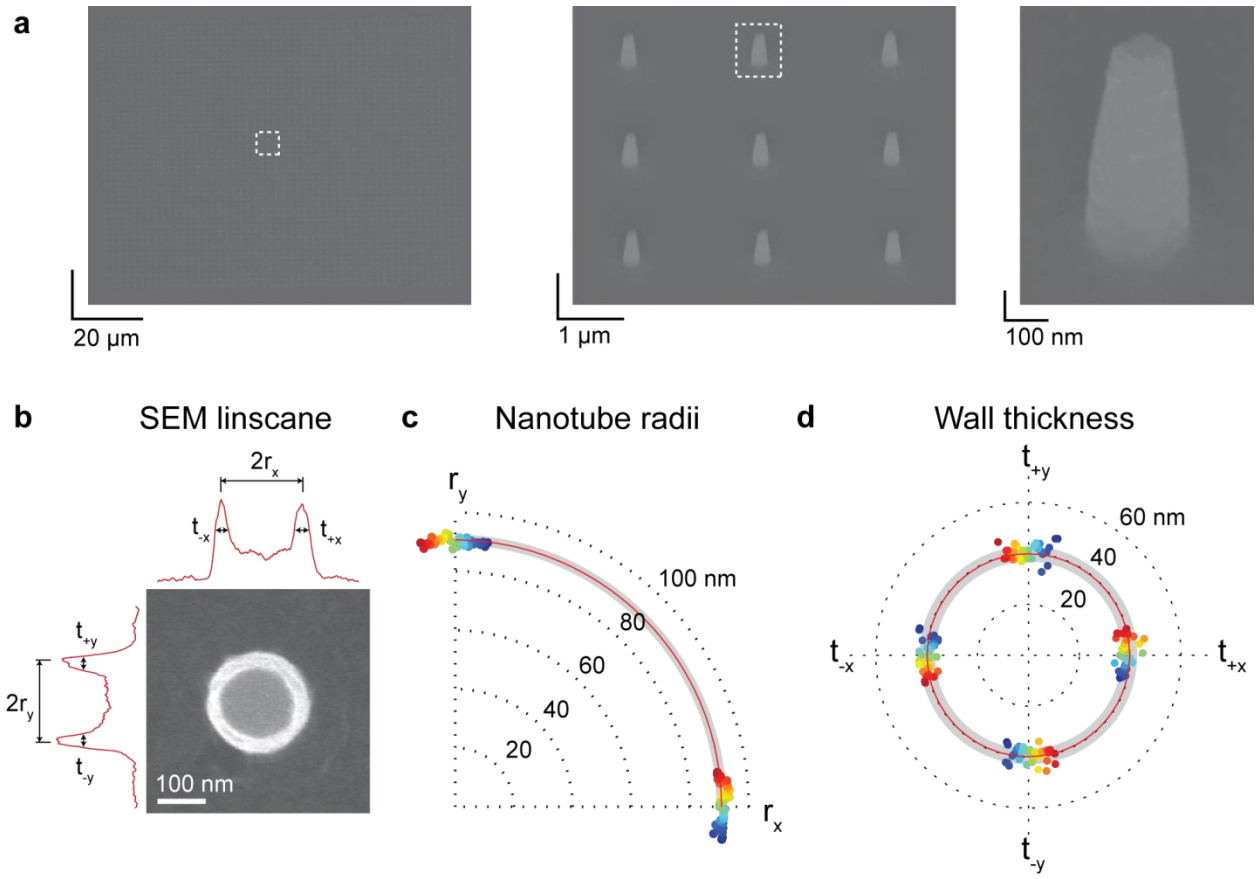

Supplementary Figure 2 | SEM characterization of electrodeposited IrOx nanotubes on a Au/Cr covered coverslip. a, Images of a 50 x 50 arrays of IrOx nanotubes electroplated on a coverslip, showing high uniformity in both size and shape. **b**, SEM top view and its secondary electron intensity line scans of a single IrOx nanotube with 1 nm per pixel resolution. Both the horizontal and vertical scans pass the center. **c, d**, Distribution of nanotube radii along x- and y-axes (**c**) and wall thickness measured at four directions (**d**). Data points with the same color are measurements from the same nanotube. The red lines represent the average values and the gray areas represent one standard deviation.

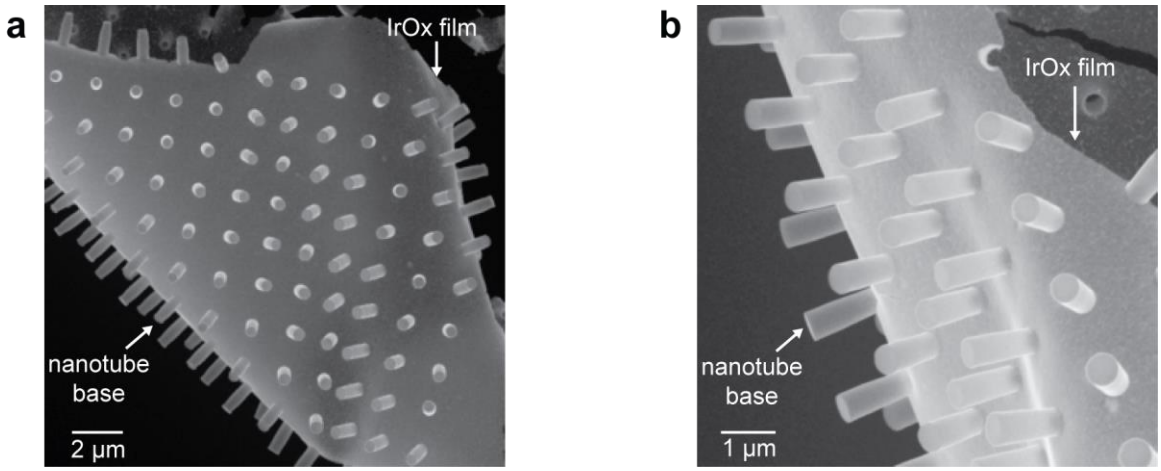

Supplementary Figure 3 | SEM images of over-electrodeposited iridium oxide nanotube arrays and films. After deposited inside the nanohole template, IrOx continued to grow and connect to form a continuous film. These films rolled over after the template removal and allowed a view of the nanotube bases. These SEM images show that the nanotubes are closed on the base ends by a layer of IrOx.

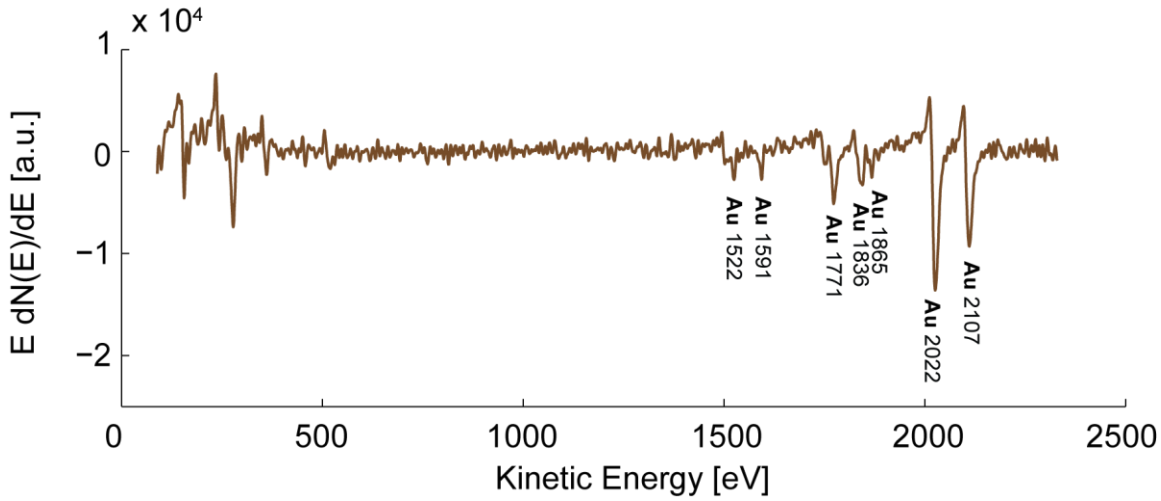

Supplementary Figure 4 | Auger electron spectroscopy of Au nanopillars.

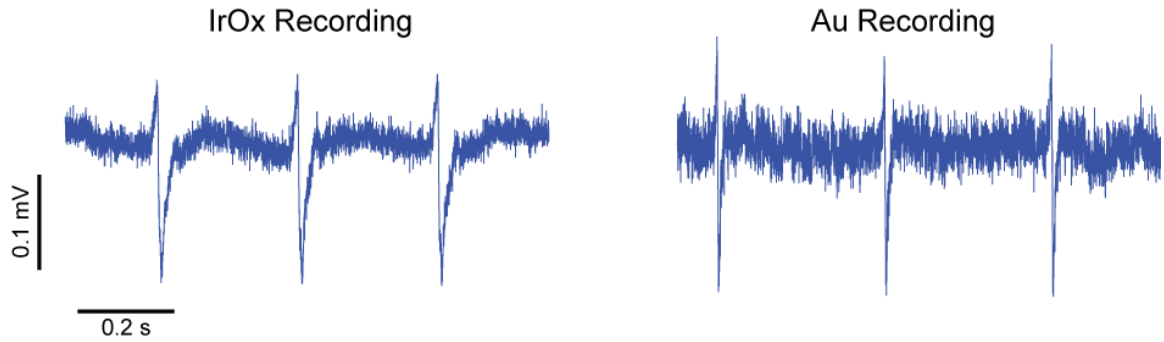

Supplementary Figure 5 | Recording of HL1 extracellular action potential by planar IrOx and Au electrodes.

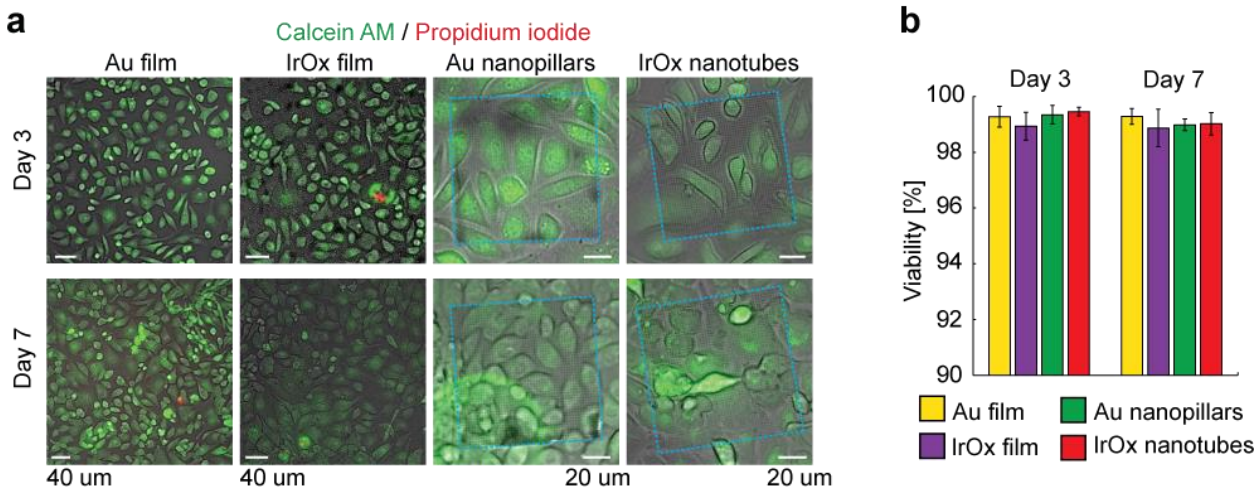

Supplementary Figure 6 | a, Fluorescent images of live HL-1 cardiomyocytes stained with calcein AM (green) and propidium iodide (red) on Au film (20 nm thickness), IrOx film (30 nm thickness on 20 nm Au film), Au nanopillar arrays (750 nm height, 180 nm diameter, 2 μm spacing on 20 nm Au film) and IrOx nanotube arrays (750 nm height, 180 nm diameter, 40 nm thickness, 2 μm spacing on 20 nm Au film) coated with fibronectin/gelatin. Dashed-line squares indicate the position of the IrOx nanotube arrays. **b**, Viability of HL-1 cardiomyocytes on 3 or 7 days (n > 1,400 cells in each data bar).

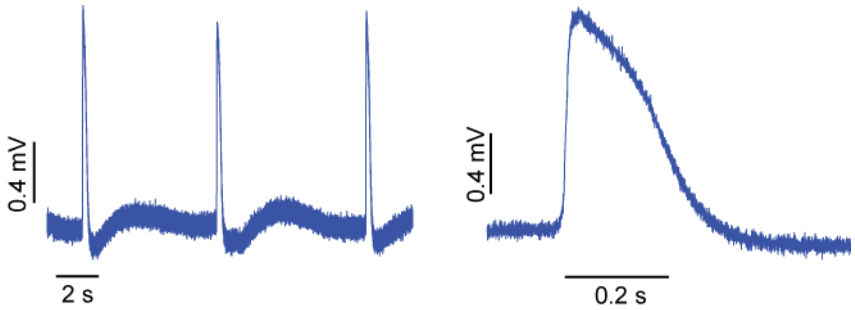

Supplementary Figure 7 | Intracellular recording of primary cultured rat cardiomyocytes by IrOx nanotube electrodes.

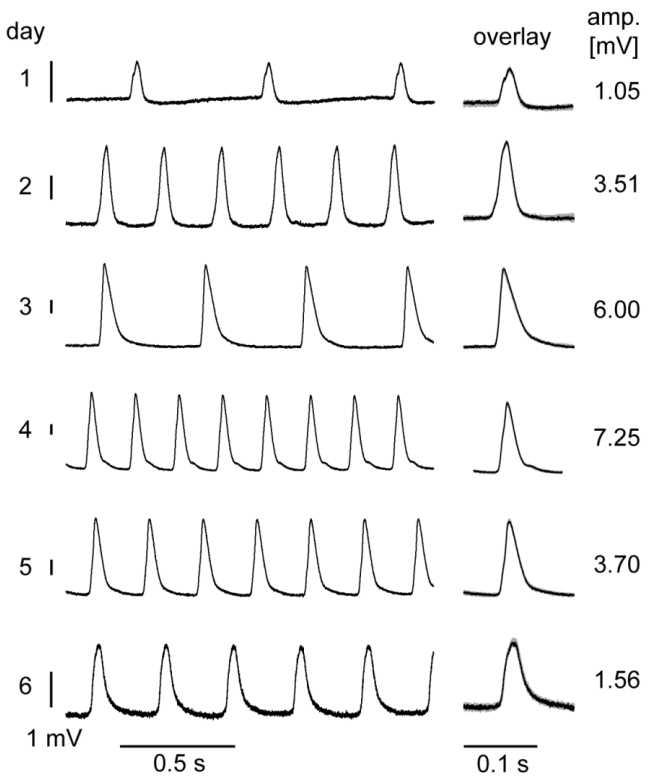

Supplementary Figure 8 | Six consecutive day recording by the same IrOx nanotube electrodes in the next culture following Fig. 3g.

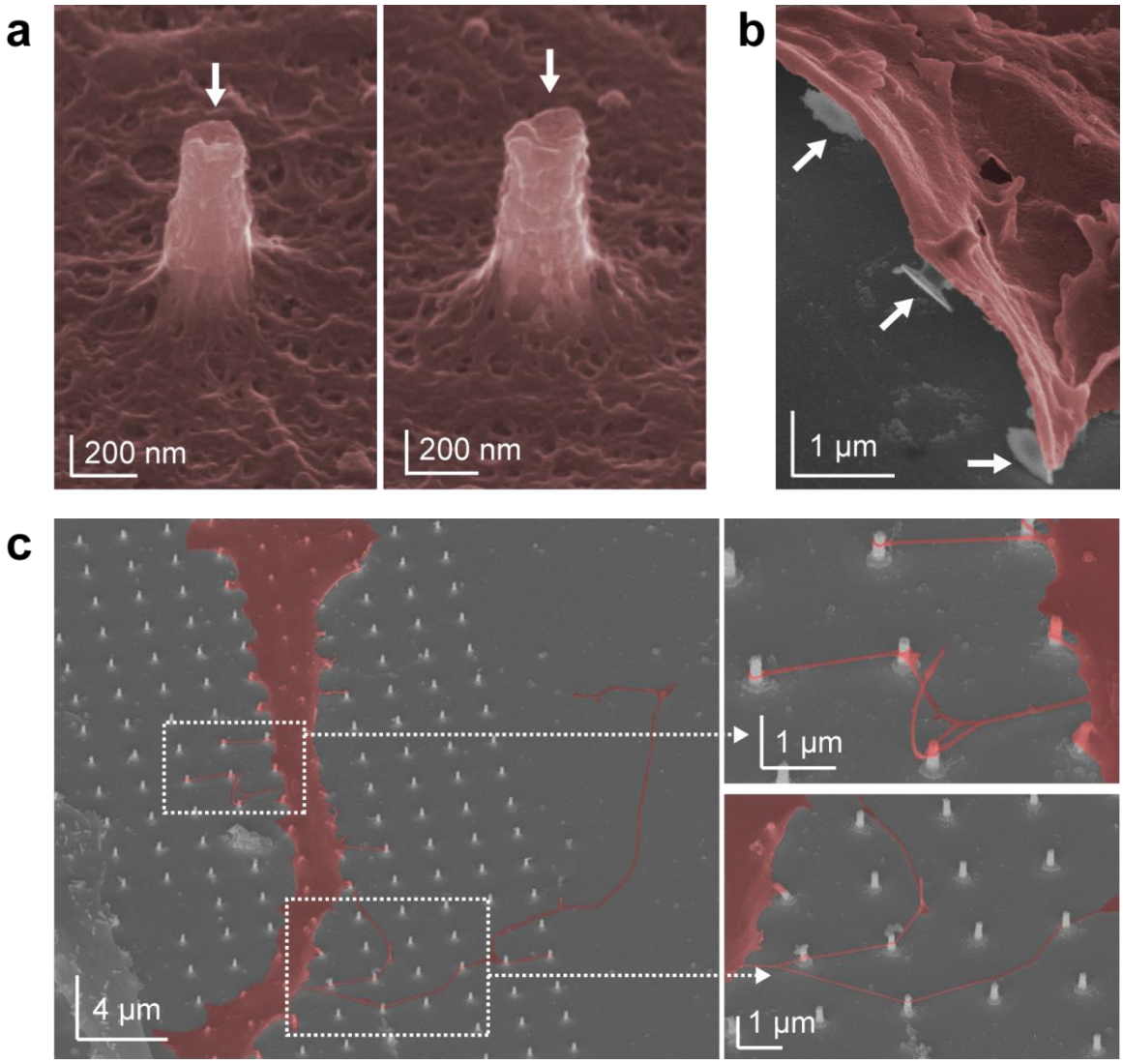

Supplementary Figure 9 | Additional SEM images of HL-1 rat cardiomyocyte interfacing with IrOx nanotubes arrays. a, Cardiomyocyte basal plasma membrane engulfs nanotubes and protrudes inside. These images were taken after the unroofing experiment. **b**, IrOx nanotubes were embedded inside a cell and unplanted from the substrate surface when the cell was partially detached during the unroofing experiment. **c**, Cardiomyocyte long protrusions tend to grab the IrOx nanotubes at the top and the waist positions.

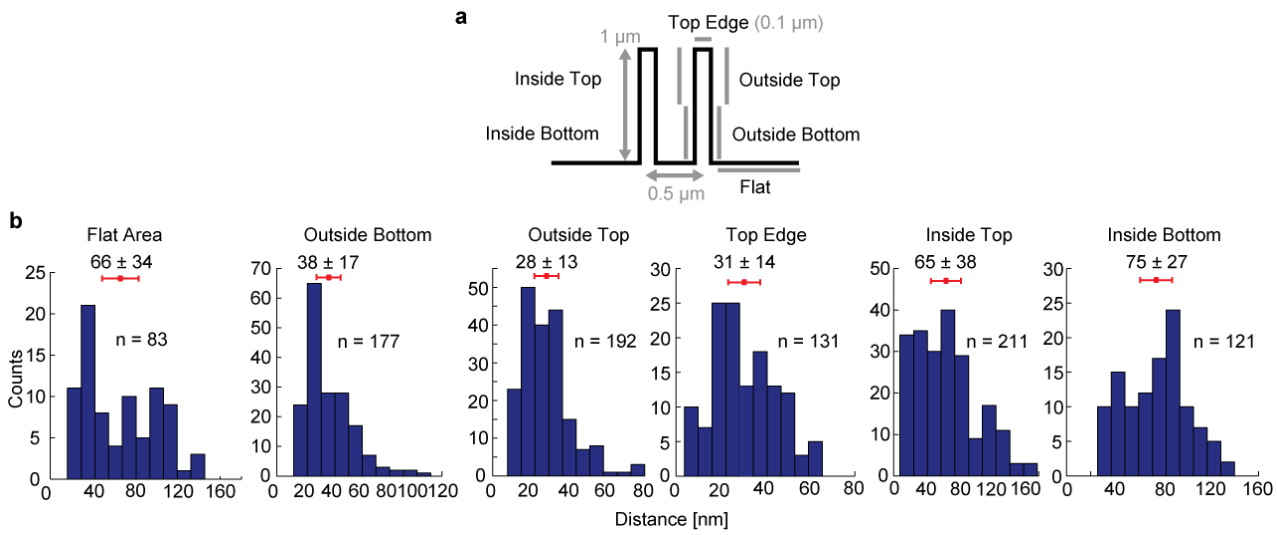

Supplementary Figure 10 | Statistics of cell membrane-quartz nanotube spacing at different regions of the nanotubes. a, Definition of regions on the nanotubes. **b**, Distance histograms of n = 12 HL-1 cardiomyocytes on 15 nanotubes. Red errorbars indicate average distances and one standard deviation.

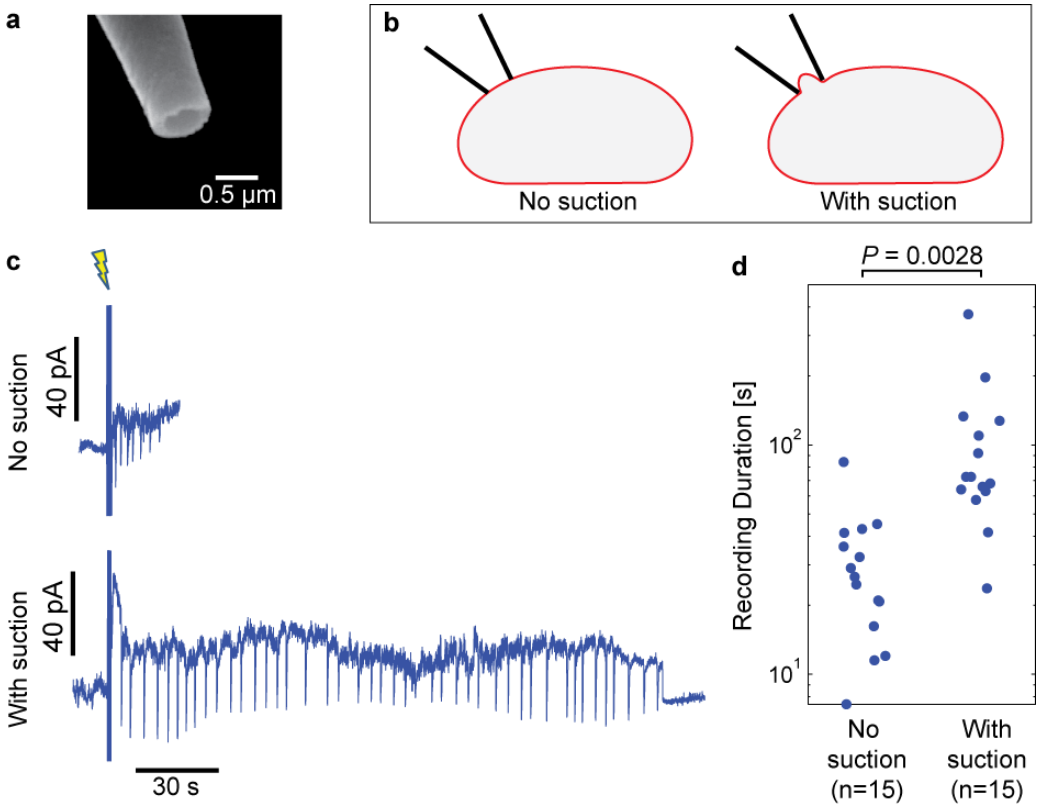

Supplementary Figure 11 | Plasma membrane curvature affects intracellular access duration after electroploration. a, SEM of patch pipette opening. **b**, Schematics illustrating the plasma membrane configuration with and without suction applied to the pipette. **c**, Trains of spontaneous action potentials recorded by patch clamp in the voltage clamp mode after electroporation. **d**, Statistics of intracellular recording duration.

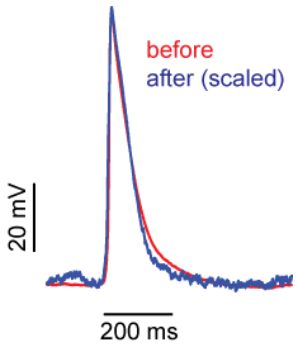

Supplementary Figure 12 | Overlay of the scaled action potentials recorded by patch clamp immediately before (red) and after (blue, scaled) IrOx nanotube electroporation.

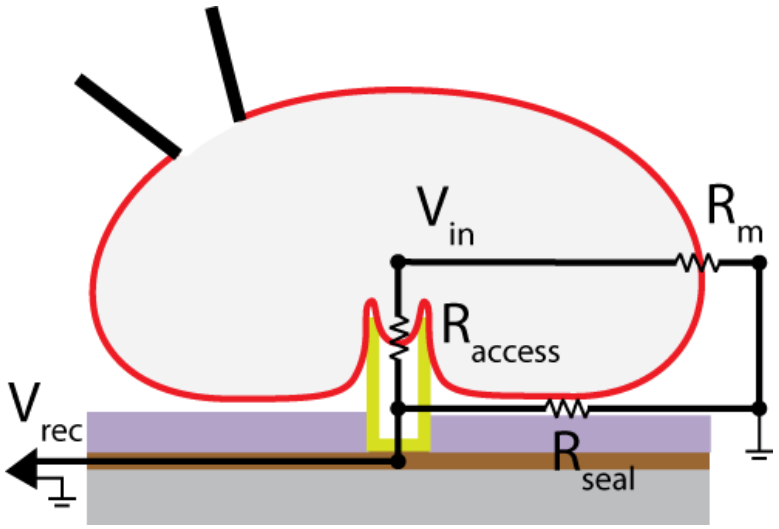

Supplementary Figure 13 | Simplified equivalent circuit diagram for cardiomyocyte-nanotube interface.

Supplementary Notes

Supplementary Note 1

Comparison between IrOx nanotube and Pt nanopillar electrodes. We previously fabricated electrodes consisted of three-by-three arrays of Pt nanopillar using focused ion beam Pt deposition[12]. The nanopillars were of 150 nm in diameter and 1.5 - 2 μm in height, which is different from the IrOx nanotubes of 180 nm in diameter and ~500 nm in height presented in this paper. Although both types of electrode are capable of recording action potentials of similar amplitudes, the Pt nanopillar electrodes achieve intracellular access for only less than two minutes[12], similar to that of the electrodeposited Au nanopillar electrodes. The IrOx nanotube electrodes possess 1-2 orders of magnitudes longer intracellular access duration.

Supplementary Note 2

Relationship between recording amplitude and pore conductance. The recorded signal $V_{rec} = V_{in}R_{seal} / (R_{seal} + R_{access})$, where V_{in} is the membrane potential, R_{seal} the sealing resistance, and R_{access} the access resistance between the nanotube electrodes and the cell interior. In most of our recordings, $R_{access} > R_{seal}$ and our recorded signal is only a fraction of the actual membrane potential. Since the access resistance is governed by the pores created by electroporation, we substitute the pore conductance $g_{pores} = R_{access}^{-1}$ and take the approximate $V_{rec} = V_{in}R_{seal} / R_{access}$ to obtain $V_{rec} = V_{in}R_{seal}g_{pores}$. Therefore, $\Delta V_{rec} = V_{in}R_{seal}\Delta g_{pores}$ and the change in the recorded signal amplitude is linearly proportional to the total conductance of the pores.